Journal of Power Sources 195 (2010) 2457–2462

Contents lists available at ScienceDirect

Journal of Power Sources

journal homepage: www.elsevier.com/locate/jpowsour

Electrochemical impedance studies of AB_5-type hydrogen storage alloy

Pawel Slepski[a], Kazimierz Darowicki[a], Maciej Kopczyk[b], Agnieszka Sierczynska[b], Karolina Andrearczyk[a,*]

[a] Department of Electrochemistry Corrosion and Materials Engineering, Gdansk University of Technology, 11/12 Narutowicza Street, 80-233 Gdansk, Poland
[b] Institute of Non-ferrous Metals, Department in Poznan, Central Laboratory of Batteries and Cells, 12 Forteczna Street, 61-362 Poznan, Poland

ARTICLE INFO

Article history:
Received 9 June 2009
Received in revised form 16 October 2009
Accepted 20 November 2009
Available online 27 November 2009

Keywords:
Nickel–metal hydride electrode
Hydrogen storage alloy
Impedance
State of charge
Depth of discharge

ABSTRACT

Electrochemical impedance spectroscopy technique was used to describe behavior of AB_5-type hydrogen storage alloy. Impedance investigations were performed during cyclic voltammetry measurement and charge/discharge cycles. The comprehensive interpretation of instantaneous impedance spectra obtained in potentiostatic mode allowed further to interpret impedance results in galvanostatic mode. Proposed methodology enabled to trace electrical parameters as a function of state of charge (SOC) and depth of discharge (DOD).

1. Introduction

Despite constant development of secondary cells and fuel cells, nickel–metal hydride (Ni/MH) cells still have a significant share in the market of batteries for mobile electronic and electrotechnical devices. Features of Ni/MH cells are mainly connected with the processes that take place on metal hydride electrode. This is the reason why this material has been the object of intensive research for many years [1–8]. The basic technique used for characterizing the material's features and reactions proceeding during charging and discharging the metal hydride electrodes is the electrochemical impedance spectroscopy [9–17]. The results are interpreted mainly on the basis of processes proceeding on the electrode, the most imported being:

- charge transfer and adsorption of hydrogen atoms on active regions of the surface (Volmer step):

$$M + H_2O + e^- \Leftrightarrow MH_{ads} + OH^- \quad (1)$$

- absorption of adsorbed hydrogen in electrode's mass:

$$MH_{ads} \Leftrightarrow MH_\alpha \quad (2)$$

- formation of the hydride β phase:

$$MH_\alpha \Leftrightarrow MH_\beta \quad (3)$$

One cannot omit the evolution of hydrogen, which proceeds during charging according to Tafel's (4) or Heyrovski's (5) mechanism:

$$2MH_{ads} \Leftrightarrow H_2 + 2M \quad (4)$$

$$MH_{ads} + H_2O + e^- \Leftrightarrow H_2 + OH^- + M \quad (5)$$

Based on the above-mentioned processes one can create different equivalent electrical circuits, allowing elements like charge transfer resistance, double layer capacitance, capacitance and resistance of adsorption, hydrogen diffusion in the electrode and other [14,15,18–22]. Unfortunately, despite many investigations, the unification of equivalent model has not yet been achieved. Moreover, it sometimes happens that time constants present in corresponding regions of impedance spectra are interpreted differently. Usually the obtained spectra have in Nyquist projection the shape of two semicircles. One of the semicircles is not always well formed and can sometimes be depressed, while the other one can have a "tail" at low frequencies. The first, high-frequency time constant is usually interpreted by the influence of the connection between current collector and electrode material, the low-frequency semicircle has its explanation in the process of charge transfer on the surface of material, while the impedance for the lowest frequencies (millihertz's)—in the process of diffusive hydrogen transport inside the material. Such interpretation is often used for determining the kinetic parameters of the processes proceed-

Abbreviations: CV, cyclic voltammetry; SOC, state of charge; DOD, depth of discharge; Ni/MH, nickel–metal hydride.

* Corresponding author. Tel.: +48 58 347 10 92; fax: +48 58 347 10 92.
E-mail addresses: corolla@chem.pg.gda.pl, bonzai@wp.pl (K. Andrearczyk).

0378-7753/$ – see front matter © 2009 Elsevier B.V. All rights reserved.
doi:10.1016/j.jpowsour.2009.11.089

ing on the electrode, e.g. current density or diffusion coefficient [23–26].

The differences and ambiguities in spectra interpretations are mostly due to the limitations of the measurement technique. Impedance measurements for metal hydride electrodes are in most cases carried out in potentiostatic mode with the use of frequency response analysis (FRA). Maintaining the stationarity conditions of the investigated system is in those cases the necessary condition. It can be achieved by "stabilizing" the electrode in order to maintain constant potential. Such approach eliminates of course the possibility to perform the measurements under real, non-stationary conditions of cell function.

The solution to this problem may be found in using impedance measurement technique with multisinusoidal perturbation and analyzing the results with short time Fourier transformation (STFT) [27,28]. The advantage of this technique over FRA is the possibility to analyze non-stationary systems and simultaneously perform impedance measurements and other techniques [29,30]. Detailed information about applying this new method in examination of electrochemical cells has been recently presented by Slepski et al. [31].

Next section presents the results of impedance measurements obtained during investigating metal hydride electrodes under the conditions of: constant-current flow and potential changing linearly.

2. Experiments

Electrodes of AB_5-type hydrogen absorbing alloys of the formula $LaMmNi_{3.55}Al_{0.3}Mn_{0.4}Co_{0.75}$ were prepared by mixing the alloy powder (<75 μm grain size) with 10 wt.% addition of nickel powder. This powder mixture was pressed at 8×10^8 Pa into ϕ 6.5 mm × 1.8 mm tablets. A pallet was then placed in a small basked of nickel gauze (current collector) and pressed again using a hand press. The experimental cell for electrochemical measurements consisted of the working electrode, the platinum counter electrode and the reference Hg/HgO/6 M KOH electrode. The electrolyte was 6 M KOH solution, and measurements were performed at room temperature. Before proper electrochemical testing working electrodes composed of metal hydride electrode (MH) were chemically preactivated by boiling in 6 M KOH solution and then the constant-current charge/discharge measurements were performed three times at current density $j = 40\ mA\ g^{-1}$. The charge process was conducted till the beginning of the hydrogen evolution on electrode. After 1 h of a rest period for potential equilibration the electrode was discharged to the potential −0.7 V.

The measurements were performed using Autolab PGSTAT 30 connected to National Instruments PXI-6120 card which generated the multisinusoidal perturbation signal.

In potentiostatic mode on linear/cyclic polarization (at sweep rate $dE/dt = 0.01\ mV\ s^{-1}$) the multisinusoidal voltage perturbation signal was added and applied by PGSTAT 30. Frequency range of this ac signal was from 4.5 kHz to 70 mHz and with 8 mV amplitude peak to peak.

In galvanostatic mode on charging/discharging current ($I = 12$ mA) the multisinusoidal current perturbation signal was added (with the same frequency range as in potentiostatic mode). Its amplitude was chosen to keep Ac components of voltage response less then 10 mV peak to peak.

The measurement's set-up and exact procedure of applying the perturbation signal, amplitude, phase shift, frequencies, resultant signal and further analysis are presented in [31]. For measurement system control, as well as further analysis, LabView applications were used.

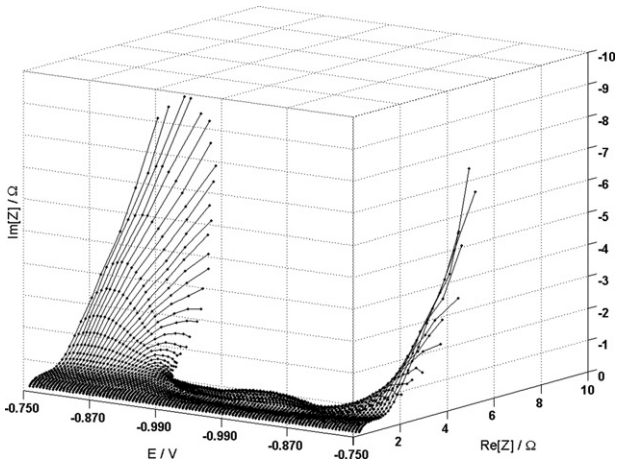

Fig. 1. MH electrode impedance changes during CV experiment.

3. Results and discussion

Fig. 1 presents the changes of the electrode's impedance and Fig. 2 the changes of current during cyclic voltammetry experiment. The results were obtained by proper analysis of current and voltage signals registered during the measurements. In Fig. 1, individual spectra have, for the lowest potentials, characteristic shape of two semicircles. The high-frequency semicircle does not change significantly, while the low-frequency semicircle evolves with the potential changes and for the highest potential it becomes a straight line.

Based on the shapes of the impedance spectra an equivalent electrical circuit was designed. It included the electrolyte resistance and elements which simulate two time constants (see Fig. 3). First constant, which corresponds to the high-frequency semicircle, is represented by resistance R_1 and a constant phase element CPE_1. The second time constant, represented by elements R_2 and CPE_2, describes the low-frequency semicircle. At this point it is worth noticing that the attempts to match the obtained impedance spectra to other models used for hydrogen electrodes analysis, which included elements corresponding to adsorption and absorption, did not give any satisfying results.

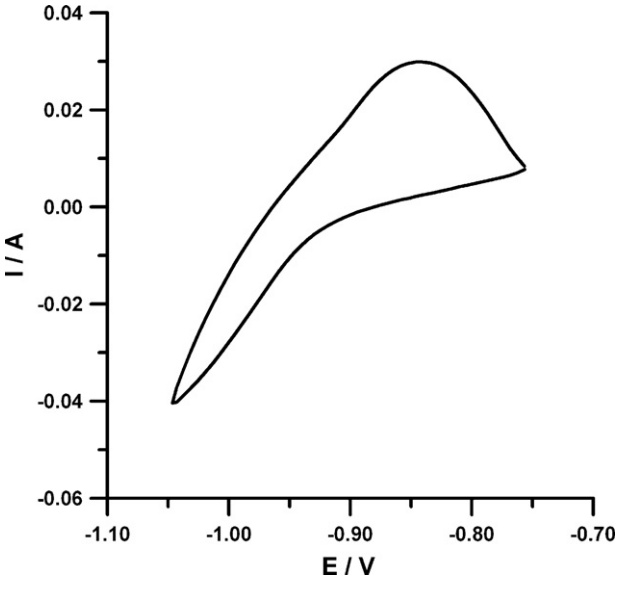

Fig. 2. Current–voltage characteristics of MH electrode.

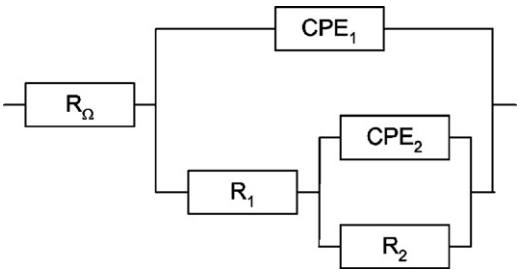

Fig. 3. Scheme of equivalent electrical circuit used for impedance spectra analysis.

The impedance of constant phase element, defined as:

$$\mathrm{ZCPE} = [Q(j\omega)^n]^{-1}, \quad (6)$$

where Q is the admittance $(1/Z)$ at 1 rad s^{-1}, this element describes the non-ideal behavior of the capacitance, j is the imaginary number, $\omega = 2\pi f$ is the angular frequency (rad s^{-1}) and the exponent $n \in \langle 0,1 \rangle$, is often used instead of capacitance in impedance analysis. Using CPE is generally related to the depressed shape of impedance spectra resulting from: porous potential distribution effect, large double layer capacitance, porosity and inhomogeneity [32–34].

R_1 and Q_1 do not change significantly with potential (less than 15%), which implies that these elements are not connected with electrochemical processes. The presence of high-frequency time constant should be therefore associated with other effects, e.g.: resistance–capacitance characteristic between reference and working electrode, connection between current collector and electrode material, features of metal hydride surface layer, etc. [19,35].

Fig. 4 presents the changes of Q_2 (Fig. 4a) and R_2 (Fig. 4b) parameters during the cathodic polarization of the electrode. Up to about −780 mV the resistance cannot be determined. Changing the potential towards more negative values initially results in decrease of both Q_2 and R_2 parameters. This tendency maintains till about −800 mV, when Q_2 reaches its minimum and R_2—the plateau. It is the range of positive overpotentials, but the changes of parameters should not be associated with the process defined in (1), since the electrode does not yet contain hydrogen that could oxidate.

For potential in range from −800 mV to about −890 mV the decrease of R_2 can be observed, while Q_2 reaches maximum and then decreases too. This is already the cathodic range and the increase of current as well as the decrease of resistance allow to associate R_2 with charge transfer resistance. Moreover, it can be assumed that only activation control takes place and the diffusion processes, related to phenomena defined by (2) and (3), are rapid enough to be omitted. These assumptions allow us to interpret the changes of Q_2 as the result of changing double layer capacitance. Further cathodic polarization results in slower decrease of both elements' values. After reaching −950 mV, a slight increase of Q_2 can be observed, while R_2 remains constant. The reason for this behavior is the limited rate of hydrogen transport inside the electrode material (the diffusion coefficient is about 10^{-8} cm^2 s^{-1} and depends on hydrogen content [25,36]). Formed in reaction (1) hydrogen having difficulties in transport inside electrode material adsorbs on the surface and as a consequence reduces the active surface. Charge transfer resistance stops decreasing, it will increase with time. At this point it is necessary to remind that the attempts to modify the equivalent circuit by adding elements corresponding to capacitance or resistance of adsorption resulted in lower rate of matching between simulated and measured impedance spectra. One of the probable causes of the mismatching is the fact that hydrogen adsorption during MH electrode charging should be considered as a process proceeding parallel with charge transfer. In that case the frequency range used in experiments would not allow the separation of the two processes and the capacitance and resistance elements would be the resultant of both of them.

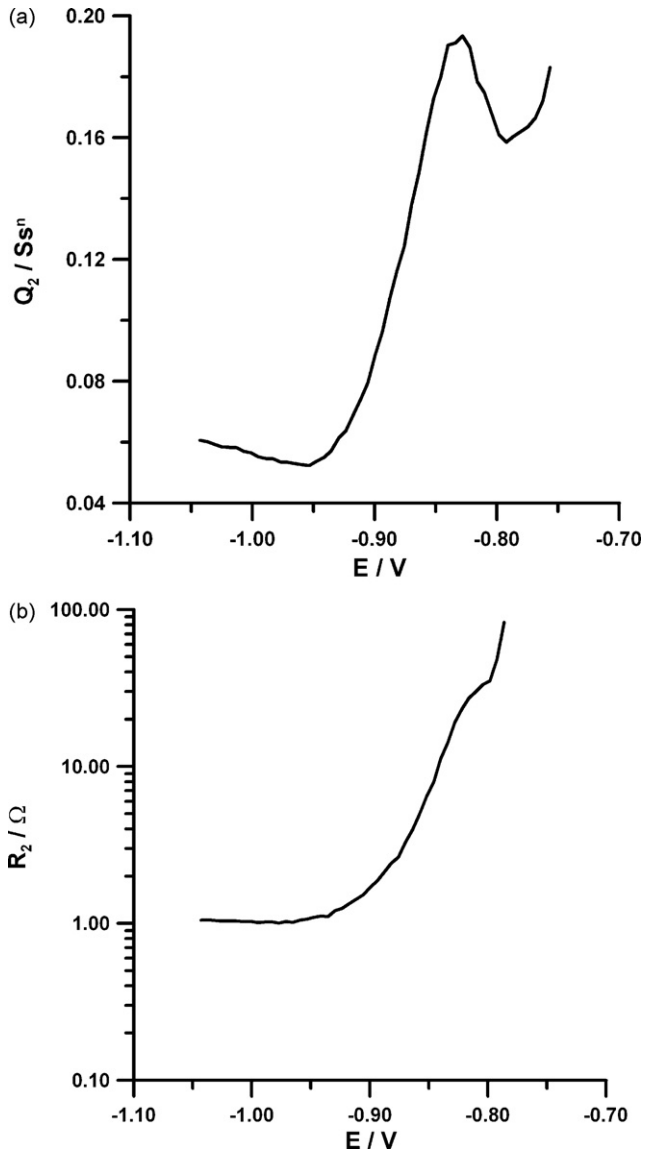

Fig. 4. (a) Changes of Q_2 parameter during linear cathodic polarization. (b) Changes of R_2 parameter during linear cathodic polarization.

The limitation of hydrogen transport inside the electrode should also cause rapid increase of imaginary values of impedance spectra for low frequencies. The absence of this effect in measured spectra can be explained by the limited frequency range of multisinusoidal signal used for the experiments. In order to maintain pseudo-stationarity within the analysis window the lowest frequency was 70 mHz, which did not allow the detection of diffusion when it is not a dominating process.

Fig. 5 presents the changes of parameters, which describe the low-frequency semicircle, during anodic polarization of the electrode. The values of Q_2 and R_2 slightly increase up till −960 mV, which is still in the range of cathodic reaction. The increase is related to constantly slowing down hydrogen reduction. Above −960 mV R_2 starts to decrease and reaches its minimum at about −870 mV. It can be explained by increasing overpotential of oxidation reaction, which results in the decrease of charge transfer resistance. For potentials above −870 mV Q_2 and R_2 increase faster. The registered current reaches its maximum and then starts to drop. The reason for this behavior is the change of process

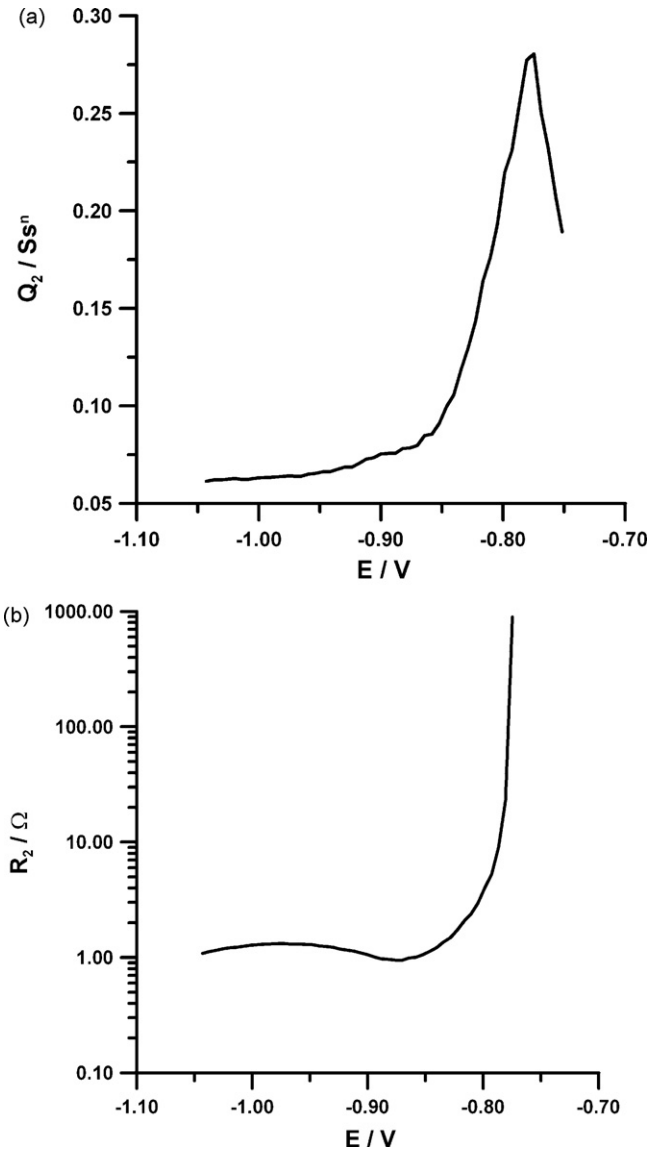

Fig. 5. (a) Changes of Q_2 parameter during linear anodic polarization. (b) Changes of R_2 parameter during linear anodic polarization.

control from activation to diffusion, which is the consequence of limited transport of reacting substances or reaction products. In the examined case the above-mentioned changes are the result of hydrogen transport from inside to the surface of the electrode. The detection of R_2 resistance is possible only for potentials lower than −780 mV. For higher potentials the shape of impedance spectra for low frequencies is a straight line.

Presented in Figs. 4 and 5 changes of parameters as a function of potential are a perfect base for interpreting the impedance spectra obtained during constant-current charging/discharging of MH electrodes. In Fig. 6 the changes of impedance during charging process are presented.

Similarly to the impedance spectra obtained during CV experiment the first, high-frequency semicircle does not change significantly. Fig. 7a and b presents SOC and the evolution of Q_2 and R_2 parameters as a function of potential changing during electrode charging. One can observe linear increase of Q_2 and a slight increase of R_2. These changes correspond to the results obtained during CV experiment (see Fig. 4). Therefore, it can be assumed that charging proceeds under the conditions of limited hydrogen transport from the surface inwards the electrode material. Electrical parameters

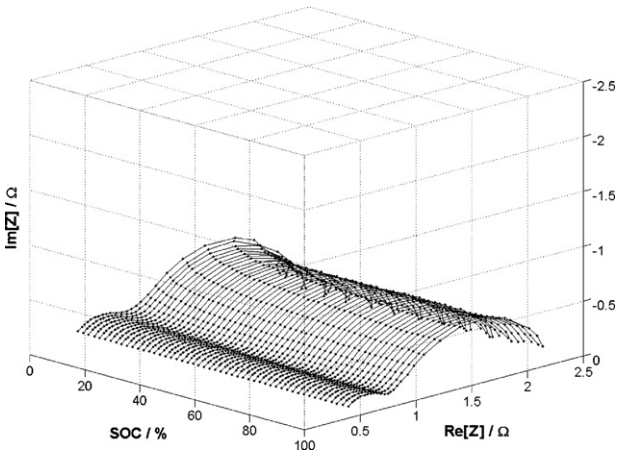

Fig. 6. Changes of MH electrode impedance during constant-current charging.

Q_2, R_2 can be associated with double layer capacitance and charge transfer resistance, respectively. However, it should be reminded that contribution of adsorption capacitance and resistance is also possible.

In Fig. 8 impedance spectra obtained during MH electrode discharging are plotted. In the initial stage of discharging,

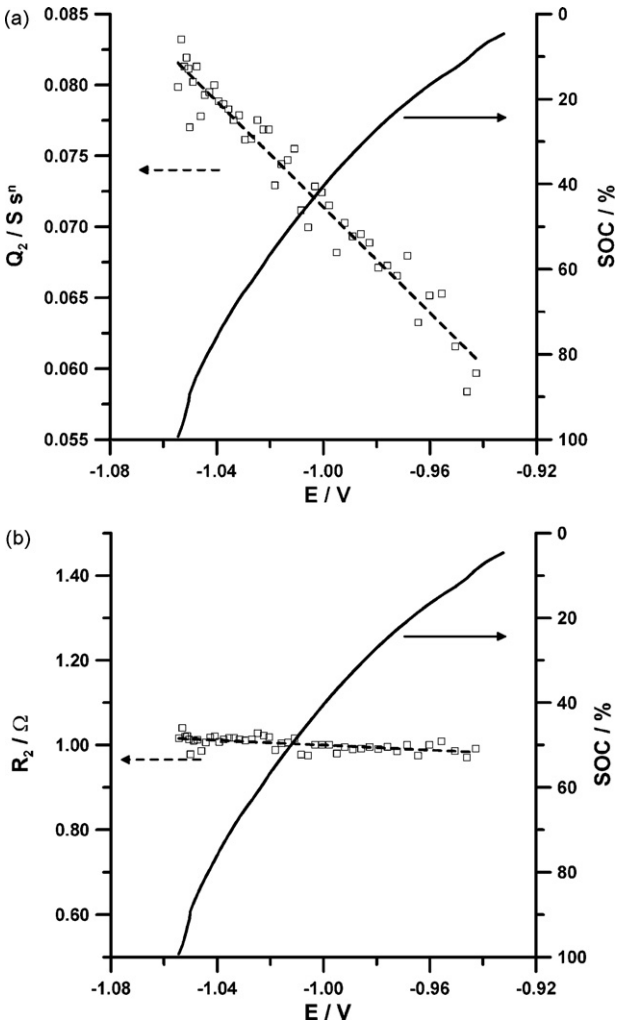

Fig. 7. (a) Changes of Q_2 parameter during constant-current MH electrode charging. (b) Changes of R_2 parameter during constant-current MH electrode charging.

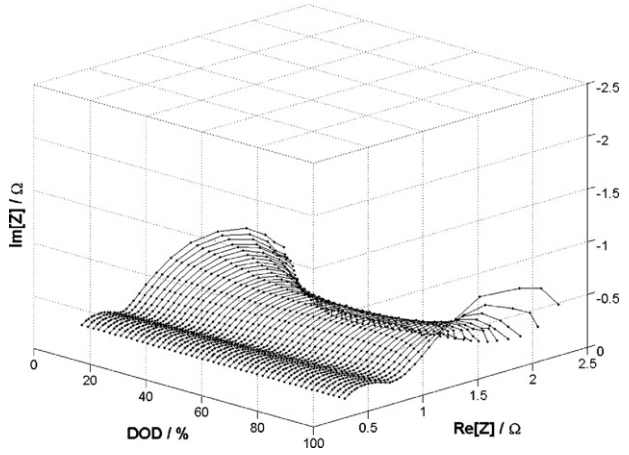

Fig. 8. Changes of MH electrode impedance during constant-current discharging.

as well as at the end of it, significant changes of impedance can be observed for low frequencies, related to the second semicircle.

The changes of electrical parameters representing this range are presented in Fig. 9. During electrode discharging both Q_2 and R_2 initially decrease. For DOD ranging from 20% to 80% the values of these parameters stabilize. Further electrode discharging results in fast increase of Q_2 and R_2.

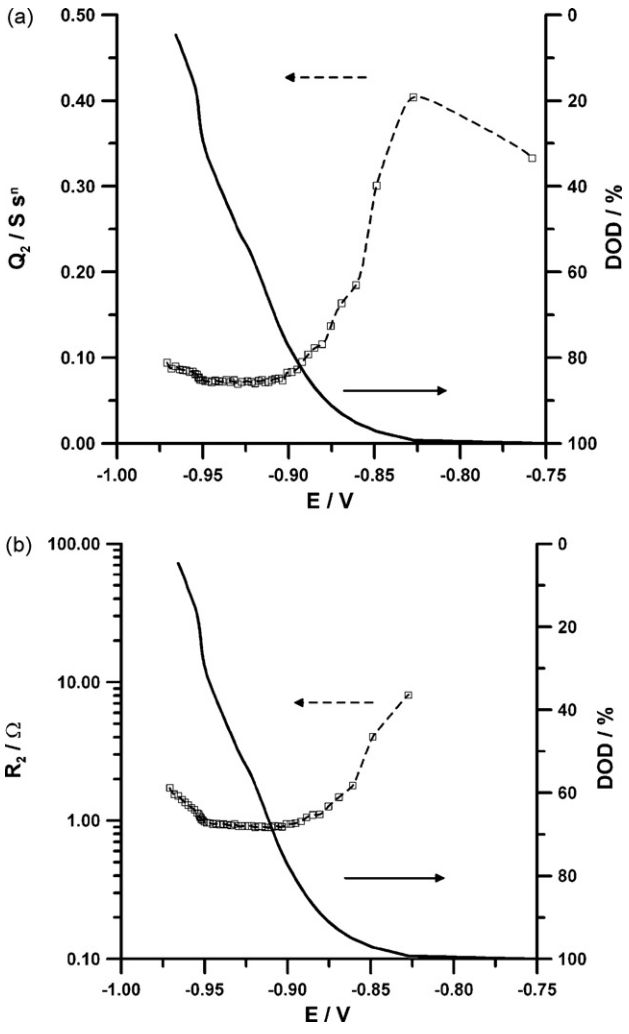

Fig. 9. (a) Changes of Q_2 parameter during constant-current MH electrode discharging. (b) Changes of R_2 parameter during constant-current MH electrode discharging.

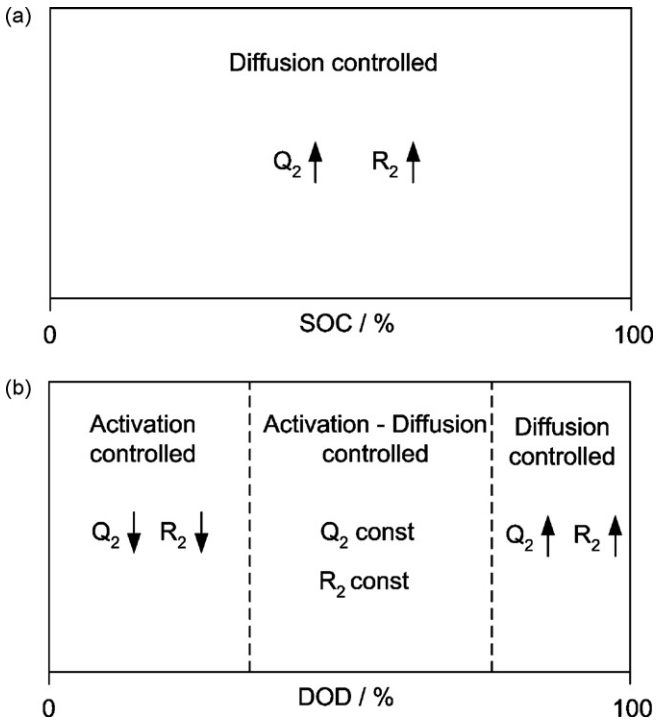

Fig. 10. (a) Scheme of relationship between reaction mechanism and impedance results as a function of SOC. (b) Scheme of relationship between reaction mechanism and impedance results as a function of DOD.

Comparing the above results with the results of CV experiment one can observe the analogy in the behavior of R_2 parameter, which in our case, represents charge transfer resistance. The initial changes caused by discharging result in the increase of potential towards more positive overpotentials. Under the activation control, this causes the decrease of charge transfer resistance. Further discharging results in the decrease of hydrogen content in electrode's mass and, as a consequence, the decrease of the speed of hydrogen transport to reaction surface [37,38]. The reaction control is switched from activation to diffusion, resulting in, i.e. the increase of charge transfer resistance.

Somewhat different behavior can be observed while comparing the initial changes of Q_2 parameter in both experiments. Probably the differences in the character of capacitance changes in the first stage of the process are the result of using constant-current instead of potential control. The decrease of Q_2 in the first stage of discharging is most likely the result of the changes of adsorption capacitance and double layer capacitance. Above 80% DOD charge transfer is much faster transportation process, therefore it should be assumed that the adsorption capacitance does not influence Q_2.

4. Conclusions

The proposed impedance method based on the multifrequency perturbation signal imposed on the investigated system showed the changes of impedance spectra as a function of potential. Obtained impedance spectra consist of two time constants. The first time constant, localized in high-frequency range, does not change regardless of the potential range. The nature of such behavior cannot be explained by electrochemical process. The second, low-frequency one, is mainly connected to charge transfer resistance and double layer capacitance. The comprehensive interpretation of impedance spectra in potentiodynamic mode allowed

further to interpret the impedance spectra during discharging/charging (in galvanostatic mode). The changes of parameters Q_2 and R_2 with SOC increase result in limited transport control of hydrogen from surface inwards electrode material—Fig. 10a. In case of discharging activation control has place. At about 80% of DOD diffusion control appears which causes sudden increase of R_2 and Q_2 parameters—Fig. 10b. Obtaining such an impedance characteristic could not be possible by using the commonly known electrochemical impedance spectroscopy, because of non-stationary conditions, the long time of measurement during which the changes of physicochemical properties occur—especially at the beginning and at the end of charging/discharging as a result of which the obtained impedance spectra by common impedance method may be questionable. The application of the proposed methodology can in the future provide useful information about the different electrode materials and about operating conditions which will be necessary for further development of Ni/MH and others batteries.

Acknowledgements

The authors acknowledge the financial support from the Ministry of Science and Higher Education (Poland) under Grant N N209 344837.

References

[1] B. Huang, P. Shi, Z. Liang, M. Chen, Y. Guan, J. Alloys Compd. 394 (2005) 303–307.
[2] R.C. Ambrosio, E.A. Ticianelli, Surf. Coat. Technol. 197 (2005) 215–222.
[3] Y. Liu, S. Zhang, R. Li, M. Gao, K. Zhong, H. Miao, H. Pan, Int. J. Hydrogen Energy 33 (2008) 728–734.
[4] M. Geng, F. Feng, S.A. Gamboa, P.J. Sebastian, A.J. Matchett, D.O. Norrtwood, J. Power Sources 96 (2001) 90–93.
[5] J.J. Reilly, G.D. Adzic, J.R. Johnson, T. Vogt, S. Maukerjee, J. McBreen, J. Alloys Compd. 293–295 (1999) 569–582.
[6] J. Kleperis, G. Wójcik, A. Czerwiński, J. Skowroński, M. Kopczyk, M. Beltowska-Brzezinska, J. Solid State Electrochem. 5 (2001) 229–249.
[7] C. Wang, M.P. Soriaga, S. Srinivasan, J. Power Sources 85 (2000) 212–223.
[8] C. Iwakura, K. Fukuda, H. Senoh, H. Inoue, M. Matsuoka, Y. Yamamoto, Electrochim. Acta 43 (1998) 2041–2046.
[9] N. Kuriyama, T. Sakai, H. Miyamura, I. Uehara, H. Ishikawa, J. Alloys Compd. 192 (1993) 161–163.
[10] S.E. Johnsen, G. Lindbergh, A. Lundqvist, R. Tunold, J. Electrochem. Soc. 150 (2003) A629–A637.
[11] X. Yuan, N. Xu, J. Alloys Compd. 329 (2001) 115–120.
[12] S.N. Begum, V.S. Muralidharan, C.A. Basha, J. Alloys Compd. 467 (2009) 124–129.
[13] E.B. Castro, S.G. Real, A. Bonesi, A. Visintin, W.E. Triaca, Electrochim. Acta 49 (2004) 3879–3890.
[14] A.M. Svensson, L.O. Valoen, R. Tunold, Electrochim. Acta 50 (2005) 2647–2653.
[15] L.O. Valoen, A. Lasia, J.O. Jensen, R. Tunold, Electrochim. Acta 47 (2002) 2871–2884.
[16] S.J. Qiu, H.L. Chu, Y. Zhang, L.X. Sun, F. Xu, Z. Cao, Int. J. Hydrogen Energy 33 (2008) 7471–7478.
[17] L.O. Valoen, R. Tunold, J. Alloys Compd. 330–332 (2002) 810–815.
[18] X. Li, H. Dong, A. Zhang, Y. Wei, J. Alloys Compd. 426 (2006) 93–96.
[19] N. Kuriyama, T. Sakai, H. Miyamura, I. Uehara, H. Ishikawa, T. Iwasaki, J. Electrochem. Soc. 139 (1992) L72.
[20] L.O. Valoen, S. Sunde, R. Tunold, J. Alloys Compd. 253–254 (1997) 656–659.
[21] N. Cui, J.L. Luo, J. Alloys Compd. 265 (1998) 305–310.
[22] P. Millet, P. Dantzer, Electrochem. Commun. 1 (1999) 163–166.
[23] R. Canha, E.A. Ticianelli, J. Solid State Electrochem. 8 (2004) 532–537.
[24] M. Raju, M.V. Ananth, L. Vijayaraghavan, J. Power Sources 180 (2008) 830–835.
[25] X. Yuan, N. Xu, J. Appl. Electrochem. 31 (2001) 1033–1039.
[26] B.S. Haran, B.N. Popov, R.E. White, J. Power Sources 75 (1998) 56–63.
[27] K. Darowicki, J. Electroanal. Chem. 486 (2000) 101–105.
[28] K. Darowicki, J. Orlikowski, G. Lentka, J. Electroanal. Chem. 486 (2000) 106–110.
[29] K. Darowicki, K. Andrearczyk, J. Power Sources 189 (2009) 988–993.
[30] K. Darowicki, J. Orlikowski, A. Arutunow, W. Jurczak, Electrochim. Acta 51 (2006) 6091–6096.
[31] P. Slepski, K. Darowicki, K. Andrearczyk, J. Electroanal. Chem. 633 (2009) 121–126.
[32] A. Lundqvist, G. Lindbergh, Electrochim. Acta 44 (1999) 2523–2542.
[33] N. Cui, J.L. Luo, Electrochim. Acta 45 (2000) 3973–3981.
[34] Y. Zhu, H. Pan, M. Gao, J. Ma, Y. Lei, Q. Wang, Int. J. Hydrogen Energy 28 (2003) 311–316.
[35] A. Yuan, N. Xu, J. Alloys Compd. 322 (2001) 269–275.
[36] C. Iwakura, M. Matsuoka, Prog. Batteries Battery Mater. 10 (1991) 81.
[37] K. Darowicki, P. Slepski, J. Electroanal. Chem. 547 (2003) 1–8.
[38] Z. Galus, Fundamentals of Electrochemical Analysis, PWN, Warszawa, 1976.